Langmuir

Article

pubs.acs.org/Langmuir

Laser Pulse Duration Is Critical For the Generation of Plasmonic Nanobubbles

Ekaterina Y. Lukianova-Hleb,[†] Alexey N. Volkov,[‡] and Dmitri O. Lapotko*[,†,§]

[†]Departments of Biochemistry and Cell Biology and [§]Department of Physics and Astronomy, Rice University, 6100 Main Street, MS-140, Houston, Texas 77005, United States

[‡]Department of Mechanical Engineering, University of Alabama, Tuscaloosa, Alabama 35487, United States

Supporting Information

ABSTRACT: Plasmonic nanobubbles (PNBs) are transient vapor nanobubbles generated in liquid around laser-overheated plasmonic nanoparticles. Unlike plasmonic nanoparticles, PNBs' properties are still largely unknown due to their highly nonstationary nature. Here we show the influence of the duration of the optical excitation on the energy efficacy and threshold of PNB generation. The combination of picosecond pulsed excitation with the nanoparticle clustering provides the highest energy efficacy and the lowest threshold fluence, around 5 mJ cm^{-2}, of PNB generation. In contrast, long excitation pulses reduce the energy efficacy of PNB generation by several orders of magnitude. Ultimately, the continuous excitation has the minimal energy efficacy, nine orders of magnitude lower than that for the picosecond excitation. Thus, the duration of the optical excitation of plasmonic nanoparticles can have a stronger effect on the PNB generation than the excitation wavelength, nanoparticle size, shape, or other "stationary" properties of plasmonic nanoparticles.

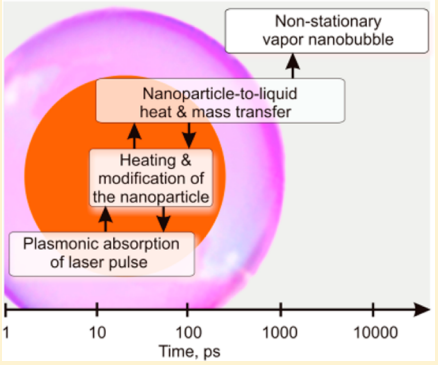

INTRODUCTION

The absorption of optical energy by micro- and nanoparticles in liquid, and the follow-up photothermal conversion and heating of the surrounding liquid, induces vapor bubbles around such particles if the incident optical fluence exceeds a specific threshold.[1−11] The energy efficacy of vapor bubble generation increases when the particle-to-liquid heat transfer is localized and the bulk heating of liquid is minimized. This thermal confinement is usually achieved by shortening the duration of the optical excitation to minimize thermal diffusion.[12] In the case of a nanoparticle, the duration of the optical excitation shortens to the nano- and picosecond range to prevent the bulk heating of the surrounding liquid.[12−14] This, in turn, makes the generation of a transient vapor nanobubble a highly nonstationary processes.[15,16] The combination of the nanosize of the optical absorber with the drastic increase in the photothermal efficacy of plasmonic nanoparticles (compared to that of any molecular absorbers) resulted in a new class of nanoevents, plasmonic nanobubbles (PNBs)—vapor nanobubbles, generated via the photothermal conversion around plasmonic nanoparticles.[4−7,9−11,15−20]

The physical properties of PNBs were shown to be different from both those of the *stationary photothermal effects* of plasmonic nanoparticles under continuous optical excitation and of laser-induced vapor bubbles in liquid via the mechanisms of *optical breakdown* or homogeneous optical absorbance by liquid. The photothermal properties of nanoparticles under stationary excitation are determined by their preset properties, such as optical absorbance, which remain permanent during their optical excitation. In contrast, an intense short pulsed excitation of metal nanoparticle during the generation of a PNB results in a rapid dynamic modification of the optical absorbance, size, structure, and phase state of the nanoparticle[21−24] and results in entirely new optical, physical, and biomedical properties of PNB compared to those of plasmonic nanoparticles.[16,22] For example, compared to gold nanospheres with a broad excitation visible spectrum, gold nanosphere-generated PNBs yield an ultranarrow peak in near-infrared.[16] The photothermal generation of vapor bubbles in optically absorbing liquids involves extensive bulk heating above the evaporation threshold temperature, while the PNB, in contrast, thermally insulates the bulk liquid and thus maintains its temperature close to the ambient level.[15] The optical breakdown-induced vapor nanobubbles do not require significant optical absorbance by the medium. However, an optical breakdown involves high local pressures and temperatures, and often shock waves, thus making it difficult to precisely control the optical breakdown-generated vapor nanobubble.[25] The relatively high threshold of laser fluence and intensity for optical breakdown limits biomedical applications of breakdown-generated nanobubbles. In contrast, PNBs demonstrated excellent biologic safety[16,20] because of their localized mechanical, nonthermal impact, and low threshold energies down to 5−15 mJ cm^{-2},[26,27] which match

Received: April 22, 2014
Revised: June 6, 2014
Published: June 10, 2014

   dx.doi.org/10.1021/la5015362 | *Langmuir* 2014, 30, 7425−7434

even the federal laser safety standards.[28] The remote on-demand generation, precise control of their mechanical impact, and easy optical and acoustic detection result in promising biomedical applications of PNBs for diagnostics, therapy, and theranostics[9,20,25−27,29−33] and in various industrial applications.[17,34,35]

However, PNB applications are still relatively limited compared to those of plasmonic nanoparticles or laser-induced vapor bubbles in liquids. This is largely caused by the lack of the universal methodology of PNB generation in real conditions. A *PNB is not a particle but rather a transient nonstationary nanoevent* that results from several transient nanoscale processes at the sub-nanosecond time scale (Figure 1). Under an excitation of plasmonic nanoparticle with an

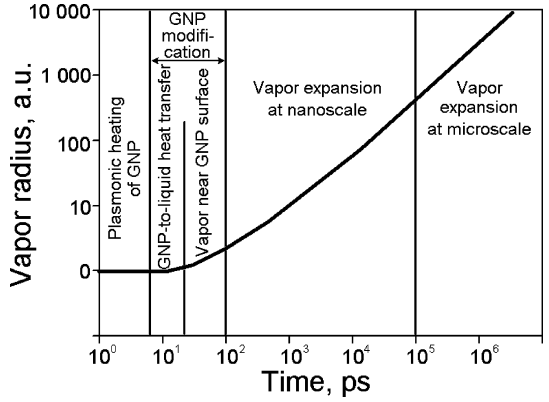

Figure 1. A temporal sequence of processes involved into the photothermal generation of plasmonic nanobubble (PNB) and the initial dynamics of the vapor layer near the surface of plasmonic (gold) nanoparticle (GNP).

ultrashort single laser, these processes include photon-phonon-heat conversion, nanoparticle surface-to-liquid heat transfer, liquid evaporation, and vapor bubble expansion and collapse. The nonstationary nature of these processes, coupled with the dynamically changing optical and thermal properties of the nanoparticle under high (melting) temperatures, seriously complicates the modeling of PNBs, compared to the modeling of stationary or low temperature photothermal effects. Experimental studies of PNBs at the nanoscale usually describe their properties under the specific duration of the excitation laser pulse and for the specific nanoparticle system. Such properties are difficult to extrapolate into other laser pulse durations and nanoparticle systems. In addition, the majority of experimental models use nanoparticle ensembles, multiple laser pulses, and indirect detection of PNBs through their secondary cumulated effects. All these factors distort the understanding of the PNB generation mechanism. As a result, the practical use of PNBs remains rather challenging for a broad community.

Here, we study the key factor for a PNB, a *duration of optical excitation*, in the range from picosecond to continuous excitation. This study employs various nanoparticle systems—from isolated nanoparticles to their suspensions and to large clusters of aggregated nanoparticles. We used the basic and most available type of plasmonic nanoparticles—solid gold nanospheres (also known as colloids)[36]—under resonant and off-resonant single pulse excitation. Individual PNBs were directly detected and quantified to provide reliable and easy-to-interpret data that can be extrapolated to various applications.

EXPERIMENTAL SECTION

Plasmonic Nanoparticles. Solid gold spherical nanoparticles (GNPs) (Vanpelt Biosciences, LLC, Montgomery Village, MD and Ted Pella, Inc., Redding, CA) were employed as a model because they showed the widest applications of the plasmonic effect. The GNPs of 60 nm diameter are also known as gold colloids. This type of GNP was invented almost 150 years ago.[36] It possesses all of the optical and thermal properties of more complex recently engineered GNPs such as rods, shells, cages, and stars. We studied three typical states of GNPs in water: single isolated particles, isolated clusters of 5−100 tightly aggregated particles, and suspensions of isolated particles. Additional GNP data can be found in the Supporting Information. The isolated particles are considered as the best model to study the PNB generation mechanism, while cluster and suspensions represent typical states of GNPs in the majority of plasmonic NP applications. GNP aggregation was achieved by adding NaCl and resuspending GNPs in water after their aggregation. The optical excitation of GNPs was performed in sealed glass cuvettes with internal lateral dimensions of 10−20 mm and a height of 0.12 mm. The cuvettes were filled with distilled water containing specific GNPs. The optical extinction spectroscopy was used to monitor the concentration of GNP suspensions (Figure S1, Supporting Information). The GNP size and shape were characterized with transmission electron microscopy (Figure S2, Supporting Information). GNP imaging is described in detail below.

PNB Generation and Detection. The results obtained with multipulse excitation can suffer from uncertainties related to the laser-induced modification of GNPs by subsequent laser pulses. In order to avoid any cumulative effects due to GNP modification and to achieve the maximum accuracy of the measurements,[10] we applied individual laser pulses of a specific wavelength, fluence, and duration. To study the resonant excitation of GNPs, the laser radiation was applied at a fixed wavelength of 532 nm, close to that of the plasmon resonance peak for 60 nm solid gold spheres. Off-resonant pulsed excitation was studied with the variable near-infrared wavelength in the range of 700−850 nm. Five excitation duration modes were realized with five lasers: 20 ps pulses (PL 2143A/20/SS, Ekspla, Lithuania), 70 ps (PL2250-1-SH-P100, Ekspla, Lithuania), 400 ps (STA-01, Standa Ltd, Lithuania), 14 ns (Lotis TII, Belarus), and a continuous laser (PGL-V-H-532, Extreme Lasers). We did not employ shorter pulses (<10 ps) in order to avoid optical breakdown and plasma formation because this regime of vapor bubble generation is completely different from the photothermal mechanism considered in the present study.[9,15,19] Tunable near-infrared wavelengths were obtained from the correspondent optical parametric generator units of each of the above-mentioned lasers. Laser beams were spatially filtered and focused into a spot of 20 μm diameter with the Gaussian spatial distribution of laser intensity. The fluence of the laser pulse was calculated from the two measured parameters. The beam diameter at the working plan was measured at the level of $1/e^2$ of the maximal fluence using the laser beam image (obtained with a CCD digital camera, Luka model, Andor Technology, Northern Ireland). The pulse energy was measured with Ophir meter (Ophir Optronics, Ltd., Israel).

Individual GNPs or their clusters and individual PNBs around them were imaged with the original time-resolved optical scattering method.[15] Briefly, a probe laser pulse (576 nm, 20 ps, 100 μJ cm^{-2}) was directed at the cuvette at a small angle (Figure 2B). Only the scattered part of the probe laser pulse was collected by the microscope objective. In order to image transient PNBs, the probe pulse was delayed with respect to the excitation pulse by 10 ns. Since the intensity of the scattered light correlates with the size of the scattering object,[15,19] the image pixel amplitude was used as a metric of the GNP cluster size. In order to estimate the PNB maximum diameter, we used another scattering technique with a low-power continuous probe laser (633 nm) (Figure 2C). This continuous probe laser was focused on the object collinearly with the excitation pulse, and the axial intensity of the probe laser was monitored. An expanding and collapsing PNB scatters the probe laser beam and, thus, reduces its axial intensity when the PNB expands and restores it to the baseline level when the PNB collapses, thus producing the signal of the PNB-specific time-shape.[15]

dx.doi.org/10.1021/la5015362 | Langmuir 2014, 30, 7425−7434

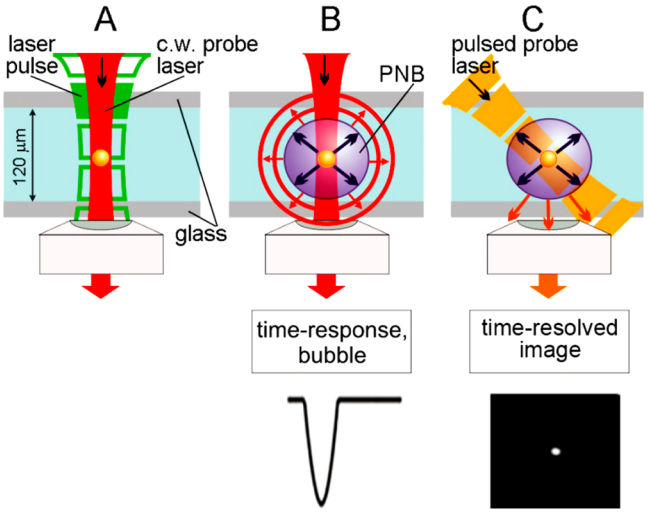

Figure 2. Schemes of experimental generation and detection of the PNB around individual GNP. (A) The GNP is exposed to a focused collinear single excitation laser pulse with tunable wavelength and fluence, and to a continuous probe laser beam (633 nm). (B) The optical scattering effect of the expanding and collapsing vapor nanobubble reduces the axial intensity of the continuous probe laser beam and thus delivers the nanobubble-specific time-response of the photodetector. (C) Optical scattering imaging of PNB with a pulsed probe laser.

The duration of the PNB-specific time-response was measured at the half-maximum level as a PNB lifetime. This lifetime correlates to the maximum diameter of the PNB[15] and therefore was used as the major PNB metric.

Modeling of the Initial Heating of a GNP Exposed to a Laser Radiation. *Pulsed Excitation.* In order to theoretically estimate the threshold fluence that corresponds to the heating of the GNP in water up to the critical water temperature and to calculate some other parameters of GNP heating, we used a model adopted from our previous work.[37] This model couples an equation with respect to the temperature of the GNP with the Navier–Stokes equations and describes the temperature and pressure distribution in the surrounding water. For the range of pulse duration under consideration, $t_L \geq 20$ ps, the effects of the electron-lattice nonequilibrium in the GNP material and thermal expansion of the GNP are relatively small and are neglected in the present model. Then the homogeneous GNP temperature, $T_p(t)$, is determined by an equation accounting for the laser heating of the GNP and its conductive cooling by the surrounding water:

$$m_p C_p \frac{dT_p}{dt} = \sigma_a I_L(t) + 4\pi r_p^2 q_f \quad (1)$$

where r_p, $m_p = (4/3)\pi r_p^3 \rho_p$, and σ_a are the particle radius, mass, and absorption cross section ($\sigma_a = 7000$ nm^2 for GNP of $r_p = 30$ nm at the laser wavelength 532 nm), $\rho_p = 19300$ kg m^{-3} and $C_p = 143.6$ J kg^{-1} K^{-1} are the density and specific heat of the particle material (gold), t is the time, $I_L(t)$ is the laser intensity, and q is the conductive heat flux density at the particle surface. The heat flux density is calculated based on the Fourier law, $q_f = -\kappa_f \partial T_f/\partial r$, at $r = r_p$, where r is the radial distance counted from the GNP center, $T_f(t,r)$ is the unsteady distribution of temperature in the surrounding fluid, and κ_f is the thermal conductivity of the fluid. In order to calculate $T_f(t,r)$ and q, eq 1 is solved together with the unsteady one-dimensional Navier–Stokes equations for compressible fluid as described in our previous work.[37] Since the purpose of the simulations is to estimate only the initial stage of GNP heating, when the vapor bubble is not formed yet, the Navier–Stokes equations are solved with the single-phase equation of state for liquid water recommended for general and scientific use by the International Association for the Properties of Water and Steam (IAPWS).[38] It is worth noting that recent molecular dynamics simulations also showed that the surface tension pressure around a 60 nm sphere can inhibit the boiling of water and thus can support further heating of the GNPs up to the bulk melting temperature of gold (1337 K) without the active expansion of a vapor bubble.[39,40] The temperature-dependent thermal conductivity and viscosity of liquid water are calculated based on tabulated data from recent IAPWS releases.[41]

In the model combining eq 1 for a GNP with the Navier–Stokes equations for the surrounding water, it is assumed that the water temperature at the GNP surface is equal to $T_p$and, thus, the effect of the finite thermal boundary resistance of the GNP/water interface is not taken into account. Other details related to the boundary conditions can be found in previous work.[37] The problem is solved numerically with a splitting method that ensures the total second order of approximation in time and space. In particular, the convective part of the Navier–Stokes equations is solved with the Richtmayer scheme, and the diffusion part is solved by the central difference scheme.[42]

In calculations of the pulsed laser heating, the temporal profile of the laser intensity is assumed to be Gaussian, $I_L(t) = F_L \exp(-[t - 3t_\sigma]^2/[2t_\sigma^2])/((2\pi t_\sigma))^{1/2}$, $t_\sigma = t_L/(2(2 \ln 2)^{1/2})$, where F_L and t_L are the incident laser fluence and the laser pulse duration (full width at half-maximum), respectively.

Continuous Excitation. In calculations of continuous wave (c.w.) laser heating, where the laser intensity is constant, $I_L = F_L/\Delta t$ (Δt is the laser exposure time), and the pressure waves are assumed to be weak and do not affect the temperature distribution in water, so that eq 1 is coupled with the one-dimensional heat conduction equation instead of full Navier–Stokes equations. In order to reveal the effects of unsteadiness during c.w. laser excitations, the computational results obtained with this model at the constant thermal conductivity of water ($\kappa_f = 0.6$ W m^{-1} K^{-1}) were compared with results obtained with a quasi-steady-state model based on eq 1, where the Fourier heat flux is calculated in the form $q_f = -2\pi R_p k_f Nu(T_p - T_\infty)$, where Nu is the Nusselt number, and T_∞ is the ambient fluid temperature. The solution of the steady-state heat transfer problem for a spherical body in a fluid with constant thermal conductivity results in $Nu = 2$.[43] With the assumption of $Nu = 2$, the solution of eq 1 takes the form:

$$T_p(t) = T_\infty + \Delta T(1 - e^{-t/\tau})$$

$$\Delta T = \frac{\sigma_a I_L}{2\pi R_p k_f Nu}, \tau = \frac{m_p C_p}{2\pi R_p k_f Nu}$$

The comparison of this solution with the numerical solution of eq 1 coupled with the unsteady heat conduction equation for water showed that the quasi-steady-state approximation ($Nu = 2$) accurately predicts the maximum increase in temperature ΔT, but substantially, in two orders of magnitude, underestimates the characteristic heating time τ.

RESULTS AND DISCUSSION

Modeling of the Initial Photothermal Response of a Gold Nanoparticle (GNP) to a Laser Pulse. To estimate how fast a vapor may develop at the surface of a GNP (60 nm solid gold nanosphere), we simulated the GNP surface temperature dynamics in water in response to a single laser pulse. In simulations, the laser fluence was fixed at the level of 66 mJ cm^{-2}, which is well above the PNB generation threshold. In this model, and for the initial stage of the GNP heating, we considered that the level of the optical absorbance cross-section of the GNP remains constant during its interaction with the laser pulse (although at later stages it changes drastically due to the GNP heating and melting). We approximated the vapor onset temperature by the critical temperature for water. This relatively high threshold ensures the onset of vapor near the GNP surface under any conditions. After this temperature level was achieved, we did not model the follow-up temperature dynamics because the laser-induced temperatures rapidly reach

dx.doi.org/10.1021/la5015362 | Langmuir 2014, 30, 7425–7434

the GNP surface melting conditions, and thus the GNP optical absorbance, structure, and size undergo radical dynamic changes.[21,22] All these dynamic changes cannot be easily incorporated into existing models.

We defined the vapor onset time t_{PNB} (Figure 3A) as the time interval from the beginning of the laser pulse (at the laser intensity level $1/e^2$) to the time point when the GNP surface temperature reaches the vapor onset threshold. Naturally, the vapor onset time cannot be shorter than the GNP thermalization time which has been approximated by 5 ps.[23,24,44,45] The vapor onset time was analyzed as a function of the laser pulse duration from 20 ps to 14 ns (black curve in Figure 3B).

We also considered continuous excitation as a separate case (see below). The shortest pulses provided the shortest vapor onset times. Formally, their values were even lower than the GNP thermalization time and were therefore approximated the vapor onset time by the longer GNP thermalization time (Figure 3B). The vapor onset time grew with the duration of the laser pulse. We further defined "the PNB energy" of the laser pulse as the percentage of the laser pulse energy, which corresponds to the time interval from the vapor onset to the end of the laser pulse (Figure 3A). This "PNB energy" indicates the incident optical energy that can be utilized by a PNB. We analyzed this PNB energy as a function of the pulse duration (red curve in Figure 3B). For picosecond pulses, the vapor onset time is only a small fraction of the whole pulse duration, and hence the level of PNB energy was relatively high. Longer pulses show a decrease in the PNB energy due to the increased thermal losses for the bulk heating of the surrounding water. Finally, we estimated the vapor onset threshold fluence which was defined as the fluence required to achieve the vapor onset temperature of the GNP surface (Figure 3C). The PNB threshold fluence increases with the pulse duration, mainly due to the increasing energy losses to the bulk heating of water. Thus, the modeled vapor onset time and the laser threshold fluence are the lowest for the shortest pulses. In particular, for the picosecond pulses the pulse energy is almost totally utilized to generate the PNB. Next, the PNBs were studied experimentally.

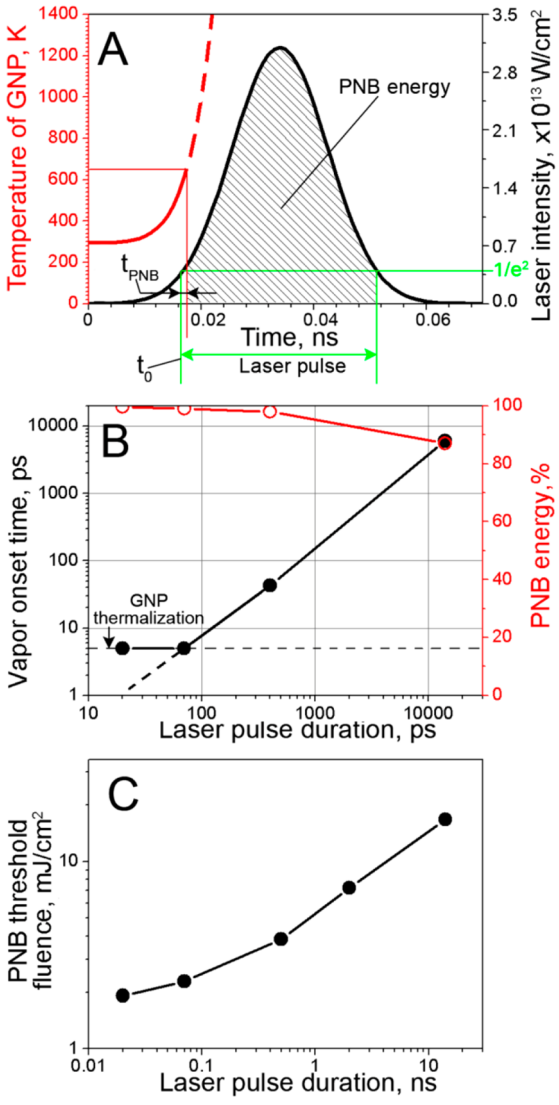

Figure 3. (A) The calculated time-course of the temperature of gold 60 nm nanospheres in water (red curve) during the absorption of a single laser pulse at 532 nm (pulse duration 20 ps) with a Gaussian temporal profile (black curve) with the fluence of 66 mJ cm^{-2}. (B) The calculated vapor onset time (black curve) and the portion of the laser pulse energy (red curve) which corresponds to the portion of the pulse after the vapor onset as a function of the laser pulse duration at 532 nm wavelength and fluence of 66 mJ cm^{-2}. (C) The calculated PNB generation threshold fluence as a function of laser pulse duration at 532 nm wavelength.

Influence of the Laser Pulse Duration on the PNB Generation Around Isolated GNPs Under Resonant Optical Excitation. To study the influence of the excitation pulse duration on PNB generation, we employed isolated GNPs in water and single laser pulses at 532 nm, which is close to the wavelength of plasmon resonance in 60 nm GNPs. Individual GNPs and PNBs were imaged via our time-resolved optical scattering method (Figure 4A,B).[19] The maximal diameter of the expanding and collapsing individual PNB was quantified through the duration of its optical scattering time-response (Figure 4C).[15] This PNB metric was applied to characterize the energy efficacy of PNB generation for a specific laser fluence. Under the fixed laser fluence applied (66 mJ cm^{-2}), PNBs were observed for all three picosecond pulse durations from 20 to 400 ps but were not observed for the nanosecond pulses (Figure 4D). The maximum PNB lifetime (and hence the maximum energy efficacy of PNB generation) was observed for the shortest pulse of 20 ps. Apparently, the fluence applied, 66 mJ cm^{-2}, was above the PNB generation threshold for 20 and 70 ps pulses, close to the threshold for the 400 ps pulse and below the threshold for the 14 ns pulse (Figure 4D). We next measured the PNB generation threshold fluence as a function of the laser pulse duration (red curve in Figure 4D).

The minimum threshold, which is less than 18 mJ cm^{-2}, was observed for the shortest, 20 ps pulse. The 20-fold increase in the pulse duration from 20 to 400 ps increases the threshold fluence 6.4-fold to 115 mJ cm^{-2}, while for the nanosecond pulse, the PNB generation threshold fluence increases by almost two orders of magnitude (red curve in Figure 4D). Thus, the laser pulse duration radically influences both the energy efficacy and the threshold fluence of PNB generation.

These experimental results qualitatively agree with the above simulations. Quantitatively, the experimentally observed PNB generation thresholds are higher than the estimated values. This disagreement may be caused by several factors that are not taken into account in the theoretical model but reduce the efficiency of PNB generation. Namely, our model does not

dx.doi.org/10.1021/la5015362 | Langmuir 2014, 30, 7425−7434

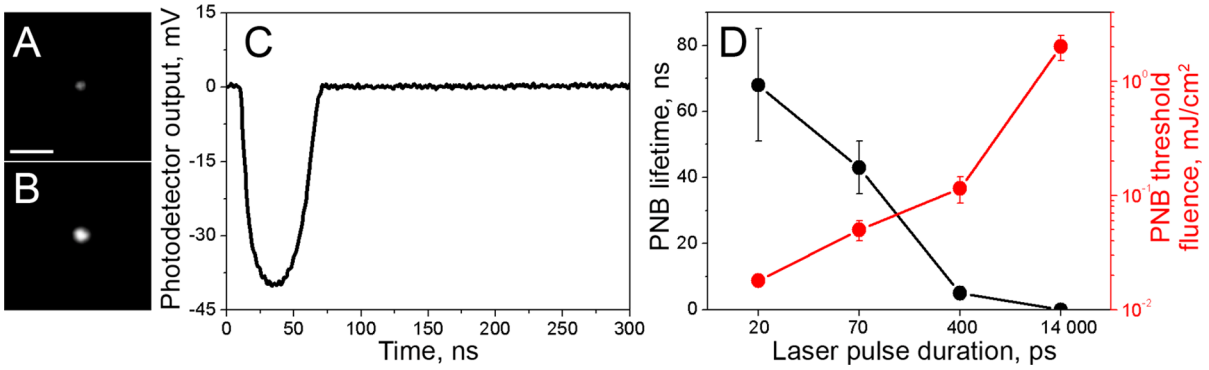

Figure 4. Generation of PNBs around isolated GNPs in water. Optical scattering time-resolved images of an individual gold 60 nm sphere in water (A) and of PNB (B) generated around the same sphere in single 20 ps pulse excitation at 532 nm. Scale bar: 2 μm. (C) Time-response of the same PNB as shown at (B) was obtained with the (continuous wave) c.w. probe laser at 633 nm. The lifetime is measured as the duration at the level of 0.5 of the maximum amplitude of the PNB-specific signal. (D) Dependences of the PNB lifetime (black curve) under specific excitation wavelength of 532 nm and fluence of 66 mJ cm^{-2} and dependence of the PNB generation threshold fluence (red curve) at the excitation wavelength of 532 nm upon the excitation duration.

account for additional energy required (1) to overcome the surface tension pressure (which is very high for isolated 60 nm GNPs), (2) to evaporate a specific volume of liquid for the formation of a PNB, and (3) to compensate a substantial dynamic decrease in the optical absorbance of a GNP during its interaction with the laser pulse. The latter effect is caused by (i) vapor around the GNP that significantly changes the dielectric functions of gold and, hence, reduces optical absorbance at the resonance wavelength,[46] (ii) extensive heating, melting, and size reduction of the GNP,[22,47−53] and (iii) additional scattering of the incident excitation laser beam by the vapor−water boundary.[15] All these factors are not taken into account in our model and explain the almost one order of magnitude difference between the theoretical and experimental PNB generation threshold fluences. A more accurate theoretical prediction of the threshold fluences requires a fairly complex computational methodology that is capable, in particular, of connecting the heat and mass transfer processes in and around a GNP with the dynamic variation of its optical absorbance. So far, such models do not exist. In addition, the individual PNB detection limit in our experiments might have been relatively high, above 200 nm, and thus the smallest PNBs (generated under the lower fluences) might have been missed. Nevertheless, the above experimental data are based on the direct detection of individual PNBs, and therefore they correctly describe the influence of the laser pulse duration on the PNB generation threshold and energy efficacy. To summarize, short picosecond pulses provide the best energy efficacy of photothermal PNB generation, while the use of popular nanosecond lasers may require a 100-fold increase in the laser energy.

GNP Ensembles vs Isolated Particles. The isolated GNPs studied above are not typical for real-world photothermal applications, where GNPs are used in the form of suspensions or/and aggregated clusters. For example, active biotargeting of GNPs results in their intracellular clustering.[20,54,55] Many industrial applications employ suspensions of GNPs.[17,34,35] We therefore studied the PNB lifetimes (a metric of the energy efficacy of PNB generation) as a function of the cluster size for isolated GNP clusters (Figure 5) and the concentration for GNP suspension (Figure 6) under a specific level of the laser fluence, 66 mJ cm^{-2}, above PNB generation threshold fluence. The excitation wavelength of 532 nm was

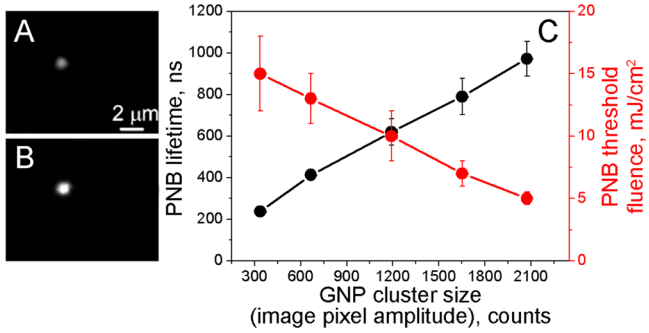

Figure 5. Generation of PNBs around isolated GNP clusters in water under resonant excitation with 20 ps laser pulse at 532 nm. Optical scattering time-resolved images of an GNP cluster in water (A) and of PNB (B) generated around the same cluster in single 20 ps pulse excitation at 532 nm. (C) The energy efficacy of PNB generation (measured via the lifetime of individual PNBs at 66 mJ cm^{-2}, black curve) and the PNB generation threshold fluence (red curve) as functions of the GNP cluster size (quantified via the pixel amplitude of the optical scattering image of a GNP cluster).

close to that of the plasmon resonance for the 60 nm solid spheres employed. On the basis of our previous results, we used the most efficient 20 ps pulse. GNP clusters in water were formed via the salt-driven aggregation of GNPs. The relative size of each individual GNP cluster was quantified via the pixel amplitude of its optical scattering image (Figure 5A). The PNB lifetime was measured for individual clusters in response to a single laser pulse (Figure 5B). The PNB lifetime increases with the GNP cluster size almost linearly and exceeds that of a single GNP by approximately five-fold (black curve in Figure 5C). This significant increase in PNB generation efficacy of the cluster vs isolated GNP under identical laser fluence can be explained by (1) the enhancement of plasmonic properties and the increased optical absorbance of the cluster,[22] (2) the coalescence of the initial vapors around GNPs into the joint vapor blanket around the whole cluster, which increases the bubble radius and hence reduces the surface tension pressure.[15] The clustering of GNPs also results in an almost four-fold decrease in the PNB threshold fluence compared to that for an isolated single GNP, from 18 mJ cm^{-2} to 5 mJ cm^{-2} (red curve in Figure 5C). This effect provides a unique opportunity to selectively generate PNBs only around the largest GNP clusters

dx.doi.org/10.1021/la5015362 | Langmuir 2014, 30, 7425−7434

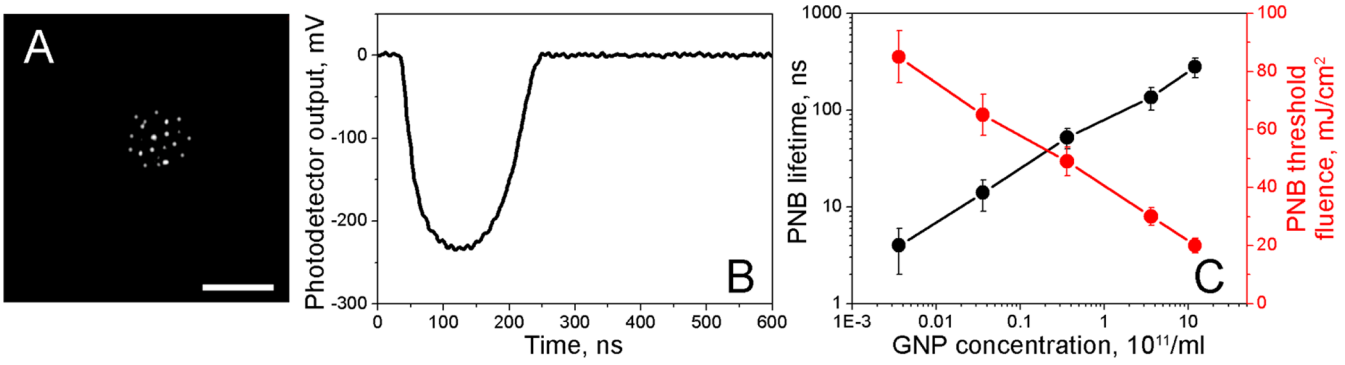

Figure 6. Generation of PNBs in water suspension of single GNPs under resonant excitation with 20 ps laser pulse at 532 nm. (A) Optical scattering time-resolved image of PNBs generated at laser fluence of 66 mJ cm^{-2}. Scale bar: 5 μm. (B) Time−response of the same PNBs as shown at (A) was obtained with the (continuous wave) c.w. probe laser at 633 nm. (C) The energy efficacy of PNB generation (measured via the lifetime of individual PNBs at 66 mJ/cm^2, black curve) and the PNB generation threshold fluence (red curve) as functions of the GNP concentration in the suspension.

at the minimum laser fluence and without generating PNBs around single unclustered GNPs or their small clusters. In biomedical applications, this cluster size effect allows a dramatic improvement in the target cell specificity of PNBs compared to that of GNPs.[20]

For water suspensions of unclustered single GNPs, we observed multiple PNBs under a single pulse excitation (Figure 6A). These multiple PNBs were generated synchronously and were analyzed through an integrated optical scattering time−response (Figure 6B). A PNB lifetime has been averaged over 10 responses obtained from 10 different areas of the suspension. An increase in the GNP concentration by four orders of magnitude increases the PNB lifetime from 4 to 280 ns (black curve in Figure 6C) and at the same time causes an almost four-fold decrease in the PNB threshold fluence (red curve in Figure 6C). Even at the maximum GNP concentration, the PNB generation threshold in suspension (20 mJ cm^{-2}) is significantly higher than that for individual GNP clusters (5 mJ cm^{-2}). Therefore, GNP clusters provide higher energy efficacy of the PNB generation compared to that for GNP suspensions.

The ensemble effects contribute to the PNB generation and detection in suspension. First, in experiments with GNP suspension, the maximum GNP concentration studied corresponds to the averaged distance between individual GNPs on the order of 1 μm. This distance is comparable with the maximum size of PNBs and may cause a coalescence of several PNBs in a larger one with a longer lifetime. Second, an increase in GNP concentration increases the probability of a single GNP being exposed to a laser pulse. In our conditions, the probability of PNB generation in suspension at the low concentration was less than 1. This influenced the averaging of the PNB lifetime over 10 pulses that were applied to the different areas of the suspension. The increase in the GNP concentration increased the PNB generation probability and, accordingly, the average lifetime. Third, at high GNP concentrations the PNB generation probability becomes equal to 1 and a further increase in the PNB lifetime is caused by the increase in the number of simultaneously generated PNBs whose integrated optical scattering effect is detected as a single time−response of a longer duration compared to that from a single PNB (in addition to the mentioned above effect of coalescence of several small PNBs into one large PNB at high GNP concentration). These three effects explain the influence of the GNP concentration upon the PNB generation energy efficacy and threshold. Therefore, the GNP suspension does not correctly describe the PNB generation mechanism for individual GNPs. Among three GNP systems studied, single GNPs, suspensions of GNPs, and clusters of tightly aggregated GNPs, the latter show the highest PNB generation efficacy.

Continuous Optical Excitation. To model the PNB generation under continuous optical excitation, we estimated the thermal response of an isolated GNP to continuous wave (c.w.) laser excitation at 532 nm under the same optical dose (fluence) as employed above for the pulsed excitation. Under the same optical dose (fluence) as employed above for the pulsed excitation, the PNB threshold temperature could not be achieved due to intense thermal losses. In this model, the duration of optical excitation was 1 s. The estimated threshold fluence turned out to be 9 orders of magnitude higher, 2×10^9 mJ cm^{-2}. Experimental studies of isolated GNPs in water under these conditions, which are identical to those described in second section for the pulsed excitation, resulted in no detectible PNBs in the range of the laser intensities below 2 MW cm^{-2} and the duration of excitation up to 20 s (fluences of up to 4×10^7 J cm^{-2}).

The GNP suspensions at the highest concentration of 10^{12} GNP per milliliter also did not return any detectable PNBs under the c.w. excitation at this laser intensity and duration as long as 60 s. When the GNP suspension was replaced by individual large (microscopically visible) GNP clusters (Figure 7A), a microscopic PNB was detected after 30 seconds of excitation at laser intensity of 2 MW cm^{-2} (Figure 7B). As the excitation was continued, PNBs grew from micro to almost macro size almost linearly with the time (Figure 7C). For isolated GNP clusters, the PNB generation threshold fluence decreased with the cluster size (Figure 7D), which was similar to what was observed under pulsed excitation (Figure 5C).

The above results show that the c.w. generation of PNBs requires multiorder increase in optical fluence compared to the pulsed excitation and in many cases cannot be achieved at all. The vapor onset times under continuous excitation are associated with a thermal diffusion radius of 12 mm (for thermal diffusion from a spherical GNP[15]), which is four orders of magnitude larger than the maximum size of a GNP cluster and more than five orders of magnitude larger than the size of an individual GNP. This spatial scale characterizes the size of the water volume heated by a GNP and clearly indicates that the c.w. laser excitation results in the bulk heating of water. In contrast, the PNB generation under short pulse excitation involves heating and evaporation of the water within several

dx.doi.org/10.1021/la5015362 | Langmuir 2014, 30, 7425−7434

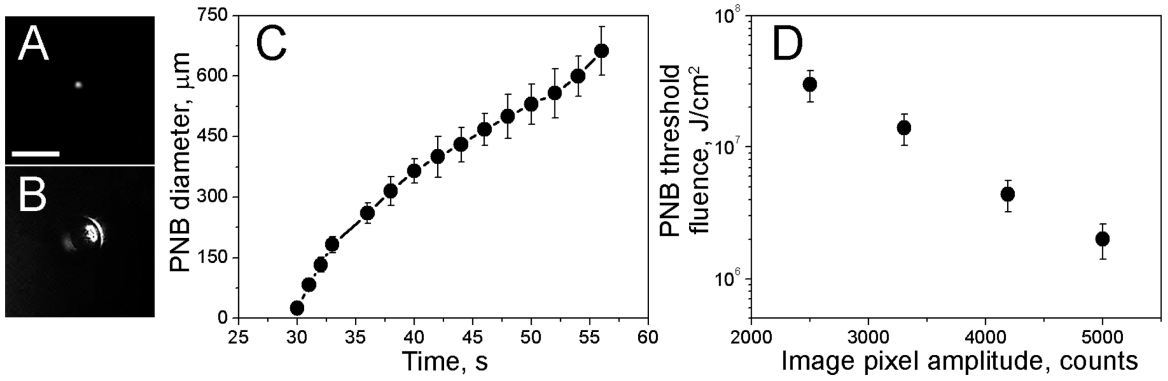

Figure 7. Continuous excitation of PNBs. Optical scattering time-resolved image of a GNP cluster (A) and PNB (B) generated around GNP cluster at the c.w. excitation (2 MW cm^{-2}, 532 nm). Scale bar: 25 μm. (C) Dependence of the PNB diameter upon continuous excitation time (532 nm), the change in the slope occurs when the bubble diameter reaches 0.12 mm, the height of the cuvette, after that, the bubble growth is basically two-dimensional. (D) PNB generation threshold fluence at continuous excitation of PNB upon the GNP cluster size quantified via the pixel image amplitude of the optical absorbance of a GNP cluster.

nanometers from GNP surface and does not affect the bulk water temperature as we observed previously.[15] The PNB generation under c.w. laser excitation, therefore, is achieved through a bulk thermal impact on the surrounding media, while the pulsed nonstationary excitation results in the localized mechanical, nonthermal impact of a rapidly expanding and collapsing PNB which, in addition, thermally insulates the bulk media from the laser-heated GNP.[15] This difference makes the c.w. generation of PNBs similar to the laser-induced generation of vapor bubbles in optically absorbing homogeneous liquid. Therefore, the advantage of plasmonic nanoparticles over optically absorbing liquids is achieved only under a short pulse excitation. In this case, the high optical absorbance of plasmonic nanoparticles efficiently supports the localized heating of the surrounding liquid above the vaporization threshold. Longer, especially continuous, optical excitation of plasmonic nanoparticles in three-dimensional liquid delocalizes their heating to macroscale. In this case, any advantage of the nanosize of optical absorbers as well as the energy efficacy, is lost, and the suspension of plasmonic nanoparticles in transparent liquid becomes almost equal to the homogeneous solution of optically absorbing liquid. In a case of planar and thermally-isolated surface, the continuous excitation of plasmonic nanoparticles[56] still may provide some localization of thermal effect. However, it cannot be a case for a PNB which is basically a three-dimensional phenomenon.

Off-Resonant Excitation. In addition to the generation of PNBs at the wavelength near the peak of plasmon resonance, we studied PNB generation at off-resonant near-infrared wavelengths in the range of 700−800 nm, far from a stationary plasmon resonance. Colloidal gold is considered to have poor optical absorbance in this spectral range, about 1% of that at the resonance wavelength at 530−540 nm.[16] The off-resonant excitation of isolated GNPs with a 20 ps pulse revealed an ultranarrow, just 3 nm wide, peak at 782 nm (Figure 8A). For gold colloids used in this experiment, the spectral width of the optical absorption spectrum is about 100 nm. Under identical laser fluence, the PNB lifetimes at 782 and 532 nm were close, thus implying that the levels of optical absorbance of GNPs at 532 and 782 nm are similar. Interestingly, we observed earlier a similar effect for longer pulses.[16] This effect is very unusual for gold colloids and has never been observed under c.w. excitation of gold nanoparticles. We therefore studied how this off-resonant effect depends upon the duration of the near-infrared laser pulse (Figure 8B). At a fixed laser fluence, 66 mJ cm^{-2}, the PNB lifetime rapidly dropped with the pulse length, and no PNBs were observed for 400 ps and 14 ns pulses. Compared to resonant excitation (Figure 4D), this unusual near-infrared peak was limited only to short picosecond pulses. It was impossible to induce PNBs with pulses longer than 70 ps under laser fluences up to 300 mJ cm^{-2}.

We further theoretically estimated the GNP surface temperature dynamics at 780 nm and determined the vapor onset times using the similar simulation approach as described above for the resonant excitation (Figure 8C). Next, based on the published data for similar GNPs,[3,4,7,27,37] we estimated that the actual expansion of a PNB does not begin simultaneously with the onset of the laser pulse (Figure 1) and may be delayed by at least 50 ps. We therefore used the time window from the vapor onset to the beginning of the active expansion of the PNB to estimate the percentage of the pulse energy that corresponds to this off-resonant PNB and determined the "off-resonant PNB energy" (Figure 8C). Upon the basis of similar calculations, this off-resonant PNB energy exceeds zero only for the short picosecond pulses of 20 and 70 ps (red curve in Figure 8B). Interestingly, the pulse duration functions of the estimated off-resonant PNB energy and the experimentally measured PNB lifetime are very close (Figure 8B). To explain this high off-resonant photothermal efficacy of gold colloids under short pulse excitation, we hypothesized earlier that a new transient plasmonic structure may emerge and exist during this short time window, and this structure transiently develops a high and narrow peak of optical absorbance at 782 nm.[16]

This hypothetical transient plasmonic structure may include hot melted gold droplets in a vapor near the surface of the parent GNP. The system of metal droplets, vapor, and the parent GNP surface may have a high optical absorbance similar to a plasmonic grating and thus efficiently convert the near-infrared pulse into a PNB. As a PNB actively expands, it mechanically destroys this structure. The coincidence of the experimental and theoretical data in Figure 8B supports the transient nature of such plasmonic structure. Its ultranarrow, 3 nm wide, peak of optical absorbance has never been reported for any isolated plasmonic structures. Furthermore, this peak is practically forbidden by electrodynamic theory, which allows for narrow spectral peaks in optical absorbance only for regular arrays and layers of plasmonic materials.[57−60] This novel, nonstationary plasmonic effect requires further in-depth

dx.doi.org/10.1021/la5015362 | Langmuir 2014, 30, 7425−7434

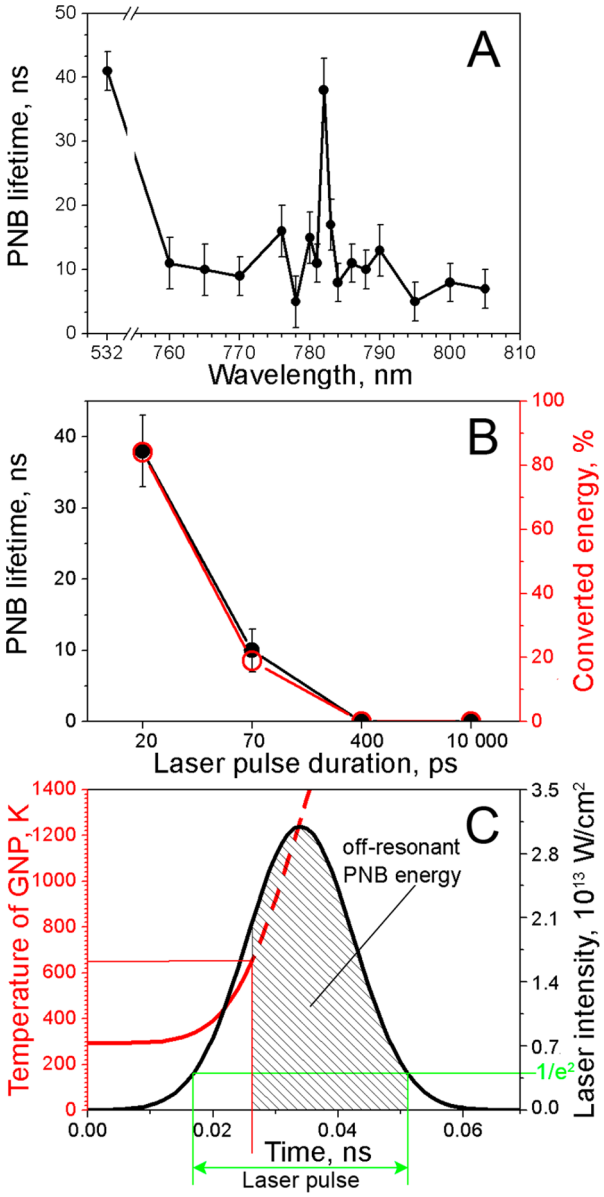

Figure 8. Off-resonant generation of PNBs around isolated individual GNPs in water obtained for 60 nm gold spheres irradiated by the 20 ps laser pulse at fluence 66 mJ cm^{-2}. (A) PNB lifetime spectra. (B) Experimentally measured PNB lifetime (black curve) and theoretically calculated off-resonant PNB energy (red curve) as functions of the duration of the excitation laser pulse at 782 nm. (C) The calculated time-course of the GNP surface temperature of (red curve) during the absorption of a single 20 ps laser pulse at 782 nm with a Gaussian temporal profile (black curve). The shaded area of the pulse shows the time window that determines the fraction of the laser pulse defined as an "off-resonant PNB energy".

studies. Nevertheless, it opens new opportunities for practical applications of plasmonic nanoparticles under "nonstationary plasmonics" and radically improves the spectral selectivity and photothermal efficacy of gold colloids at wavelength where such properties cannot be achieved under stationary plasmonic conversion.

CONCLUSIONS

In this study, we observed a nine orders of magnitude difference in the energy efficacy and threshold of the PNB generation with the variation of the duration of the optical excitation of plasmonic nanoparticles from picosecond pulses to continuous excitation. In addition, we observed a strong dependence of the PNB generation parameters upon the nanoparticle state: isolated, suspension, or clustered. Finally, we observed the unique for PNBs opportunity for the nonstationary off-resonant excitation of plasmonic nanoparticles at the wavelengths where the stationary optical properties of plasmonic nanoparticles formally exclude any efficient photothermal response. Naturally, other parameters of plasmonic nanoparticles influence the PNB generation. The influence of the GNP size on the PNB generation was extensively analyzed by us previously. Generally, the solid spheres of a smaller size or larger than 200 nm would require more fluence to generate identical PNBs under the resonant excitation.[15] The results obtained here for 60 nm gold colloids are fairly representative because the variation of the nanoparticle size in a wide range from 10 to 250 nm results in less than one order of magnitude variation in the PNB generation energy efficacy and threshold.[15,61] The shape and structure of the GNPs of similar size also influence the PNB generation energy efficacy and threshold fluence by less than one order of magnitude.[27,29,55] Therefore, the duration of the optical excitation appears to be the most critical factor in the photothermal generation of PNB compared to the GNP properties. PNB generation follows several universal rules:

(i) A PNB can be generated around a plasmonic nanoparticle using both pulsed nonstationary and continuous stationary optical excitation.

(ii) The maximum energy efficacy of the photothermal generation of PNB is achieved with picosecond laser pulses, while the minimum energy efficacy is associated with continuous optical excitation, which requires up to nine orders of magnitude more energy to generate plasmonic nanobubble, compared to picosecond laser pulses.

(iii) The clusters of aggregated nanoparticles provide the maximal energy efficacy of PNB generation compared to isolated nanoparticles or their suspensions.

(iv) For short laser pulses, generation of PNBs does not cause bulk heating of surrounding liquid, while continuous optical excitation of plasmonic nanoparticles results in an opposite effect of significant bulk heating of surrounding liquid.

(v) Short picosecond off-resonant near-infrared optical excitation of gold colloids results in efficient generation of plasmonic nanobubbles at a specific wavelength and in a very narrow, nanometers-wide, spectral interval around 780 nm.

ASSOCIATED CONTENT

Supporting Information

Figure S1. Optical extinction spectra of water suspension of GNPs. Figure S2. GNP size and shape evaluation: Transmission electron microscopy images (a) and the histogram of the GNP diameter (b). This material is available free of charge via the Internet at http://pubs.acs.org.

AUTHOR INFORMATION

Corresponding Author

*Phone: 713-348-3708; fax: 713-348-5154; e-mail: dl5@rice.edu.

Notes

The authors declare no competing financial interest.

dx.doi.org/10.1021/la5015362 | *Langmuir* 2014, 30, 7425−7434

■ ACKNOWLEDGMENTS

This work was supported in part by National Institute of Health Grant R01GM094816 and U.S. National Science Foundation Grant CBET-1341212.

■ REFERENCES

(1) Brinkmann, R.; Hüttmann, G.; Rögener, J.; Roider, J.; Birngruber, R.; Lin, C. P. Origin of Retinal Pigment Epithelium Cell Damage by Pulsed Laser Irradiance in The Nanosecond to Microsecond Time Regimen. *Lasers Surg. Med.* **2000**, *27*, 451−464.
(2) Leszczynski, D.; Pitsillides, C. M.; Pastila, R. K.; Anderson, R. R.; Lin, C. P. Laser-Beam-Triggered Microcavitation: a Novel Method for Selective Cell Destruction. *Radiat. Res.* **2001**, *156*, 399−407.
(3) Dou, Y.; Zhigilei, L. V.; Winograd, N.; Garrison, B. J. Explosive Boiling of Water Films Adjacent to Heated Surfaces: A Microscopic Description. *J. Phys. Chem. A* **2001**, *105*, 2748−2755.
(4) Kotaidis, V.; Plech, A. Cavitation Dynamics on The Nanoscale. *Appl. Phys. Lett.* **2005**, *87*, 213102.
(5) Farny, C. H.; Wu, T.; Holt, R. G.; Murray, T. W.; Roy, R. A. Nucleating Cavitation From Laser-Illuminated Nano-Particles. *ARLO* **2005**, *6*, 138−143.
(6) Inasawa, S.; Sugiyama, M.; Noda, S.; Yamaguchi, Y. Spectroscopic Study of Laser-Induced Phase Transition of Gold Nanoparticles on Nanosecond Time Scales and Longer. *J. Phys. Chem. B* **2006**, *110*, 3114−3119.
(7) Siems, A.; Webwr, S. A. L.; Boneberg, J.; Plech, A. Thermodynamics of Nanosecond Nanobubble Formation at Laser-Excited Metal Nanoparticles. *New J. Phys.* **2011**, *13*, 043018.
(8) Lapotko, D.; Lukianova, K.; Shnip, A. Photothermal Responses of Individual Cells. *J. Biomed. Opt.* **2005**, *10*, 014006.
(9) Lapotko, D.; Lukianova, E.; Oraevsky, A. Selective Laser Nano-Thermolysis of Human Leukemia Cells with Microbubbles Generated Around Clusters of Gold Nanoparticles. *Lasers Surg. Med.* **2006**, *38*, 631−642.
(10) Lukianova-Hleb, E. Y.; Lapotko, D. O. Experimental Techniques for Imaging and Measuring Transient Vapor Nanobubbles. *Appl. Phys. Lett.* **2012**, *101*, 264102.
(11) Baffou, G.; Polleux, J.; Rigneault, H.; Monneret, S. Super-Heating and Micro-Bubble Generation around Plasmonic Nanoparticles under cw Illumination. *J. Phys. Chem. C* **2014**, *118*, 4890−4898.
(12) Anderson, R. R.; Parrish, J. A. Selective Photothermolysis: Precise Microsurgery by Selective Absorption of Pulsed Radiation. *Science* **1983**, *220*, 524−527.
(13) Hu, M.; Hartland, G. V. Heat Dissipation for Au Particles in Aqueous Solution: Relaxation Time versus Size. *J. Phys. Chem. B* **2002**, *106*, 7029−7033.
(14) Link, S.; El-Sayed, M. A. Spectral Properties and Relaxation Dynamics of Surface Plasmon Electronic Oscillations in Gold and Silver Nanodots and Nanorods. *J. Phys. Chem. B* **1999**, *103*, 8410−8426.
(15) Lukianova-Hleb, E.; Hu, Y.; Latterini, L.; Tarpani, L.; Lee, S.; Drezek, R.; Hafner, J.; Lapotko, D. Plasmonic Nanobubbles as Transient Vapor Nanobubbles Generated Around Plasmonic Nanoparticles. *ACS Nano* **2010**, *4*, 2109−2123.
(16) Lukianova-Hleb, E. Y.; Volkov, A.N.; Wu, X.; Lapotko, D. O. Transient Enhancement and Spectral Narrowing of The Photothermal Effect of Plasmonic Nanoparticles Under Pulsed Excitation. *Adv. Mater.* **2013**, *25*, 772−776.
(17) François, L.; Mostafavi, M.; Belloni, J.; Delaire, J. A. Optical Limitation Induced by Gold Clusters: Mechanism and Efficiency. *Phys. Chem. Chem. Phys.* **2001**, *3*, 4965−4971.
(18) Lapotko, D.; Lukianova, E.; Shnip, A.; Zheltov, G.; Potapnev, M.; Oraevsky, A.; Savitskiy, V.; Klimovich, O. Photothermal Microscopy and Laser Ablation of Leukemia Cells Targeted with Gold Nanoparticles. *Proc. SPIE* **2005**, *5697*, 82−89.
(19) Hleb, E.; Lapotko, D. Influence of Transient Environmental Photothermal Effects on Optical Scattering by Gold Nanoparticles. *Nano Lett.* **2009**, *9*, 2160−2166.
(20) Lukianova-Hleb, E. Y.; Ren, X.; Sawant, R. R.; Wu, X.; Torchilin, V. P.; Lapotko, D. O. On-Demand Cancer Cell-Specific Plasmonic Nanobubble-Mediated Enhancement of Intracellular Drug Release and Radiation Effects. *Nat. Med.* **2014**, DOI: 10.1038/nm.3484.
(21) Hleb, E. Y.; Lapotko, D. O. Photothermal Properties of Gold Nanoparticles Under Exposure to High Optical Energies. *Nanotechnology* **2008**, *19*, 355702.
(22) Akchurin, G.; Khlebtsov, B.; Akchurin, G.; Tuchin, V.; Zharov, V.; Khlebtsov, N. Gold Nanoshell Photomodification under Single Nanosecond Laser Pulse Accompanied by Color-Shifting and Bubble Formation Phenomena. *Nanotechnology* **2008**, *19*, 015701.
(23) Link, S.; El-Sayed, M. A. Optical Properties and Ultrafast Dynamics of Metallic Nanocrystals. *Annu. Rev. Phys. Chem.* **2003**, *54*, 331−366.
(24) Hartland, G. Measurements of The Material Properties of Metal Nanoparticles by Time-Resolved Spectroscopy. *Phys. Chem. Chem. Phys.* **2004**, *6*, 5263−5274.
(25) Vogel, A.; Linz, N.; Freidank, S.; Paltauf, G. Femtosecond-Laser-Induced Nanocavitation in Water: Implications for Optical Breakdown Threshold and Cell Surgery. *Phys. Rev. Lett.* **2008**, *100*, 038102.
(26) Lukianova-Hleb, E. Y.; Oginsky, E. Y.; Samaniego, A. P.; Shenefelt, D. L.; Wagner, D. S.; Hafner, J. H.; Farach-Carson, M. C.; Lapotko, D. O. Tunable Plasmonic Nanoprobes for Theranostics of Prostate Cancer. *Theranostics* **2011**, *1*, 3−17.
(27) Plech, A.; Kotaidis, V.; Lorenc, M.; Boneberg, J. Femtosecond Laser Near-Field Ablation From Gold Nanoparticles. *Nat. Phys.* **2006**, *2*, 44−47.
(28) Laser Institute of America. ANSI Z136.1-2007, 2007.
(29) Braun, G. B.; Pallaoro, A.; Wu, G.; Missirlis, D.; Zasadzinski, J. A.; Tirrell, M.; Reich, N. O. Laser-Activated Gene Silencing via Gold Nanoshell-siRNA Conjugates. *ACS Nano* **2009**, *3*, 2007−2015.
(30) McLaughlan, J. R.; Roy, R. A.; Ju, H.; Murray, T. W. Ultrasonic Enhancement of Photoacoustic Emissions by Nanoparticle-Targeted Cavitation. *Opt. Lett.* **2010**, *35*, 2127−2129.
(31) Ibrahimkutty, S.; Kim, J.; Cammarata, M.; Ewald, F.; Choi, J.; Ihee, H.; Plech, A. Ultrafast Structural Dynamics of The Photocleavage of Protein Hybrid Nanoparticles. *ACS Nano* **2011**, *5*, 3788−3794.
(32) Peeters, S.; Kitz, M.; Preisser, S.; Wetterwald, A.; Rothen-Rutishauser, B.; Thalmann, G. N.; Brandenberger, C.; Bailey, A.; Frenz, M. Mechanisms of Nanoparticle-Mediated Photomechanical Cell Damage. *Biomed. Opt. Express* **2012**, *3*, 435−446.
(33) Arita, Y.; Ploschner, M.; Antkowiak, M.; Gunn-Moore, F.; Dholakia, K. Laser-Induced Breakdown of An Optically Trapped Gold Nanoparticle for Single Cell Transfection. *Opt. Lett.* **2013**, *38*, 3402−3405.
(34) Yuan, F.; Sankin, G.; Zhong, P. Dynamics of Tandem Bubble Interaction in a Microfluidic Channel. *J. Acoust. Soc. Am.* **2011**, *130*, 3339−3346.
(35) Zhao, C.; Liu, Y.; Zhao, Y.; Fang, N.; Huang, T. J. A Reconfigurable Plasmofluidic Lens. *Nat. Commun.* **2013**, *4*, 2305.
(36) Faraday, M. The Bakerian Lecture: Experimental Relations of Gold (and Other Metals) to Light. *Philos. Trans. R. Soc. London* **1857**, *147*, 145−181.
(37) Volkov, A. N.; Sevilla, C.; Zhigilei, L. V. Numerical Modeling of Short Pulse Laser Interaction with Au Nanoparticle Surrounded by Water. *Appl. Surf. Sci.* **2007**, *253*, 6394−6399.
(38) Wagner, W.; Pruß, A. The IAPWS Formulation 1995 for the Thermodynamic Properties of Ordinary Water Substance for General and Scientific Use. *J. Phys. Chem. Ref. Data* **2002**, *31*, 387.
(39) Merabia, S.; Keblinski, P.; Joly, L.; Lewis, L. J.; Barrat, J. L. Critical Heat Flux Around Strongly Heated Nanoparticles. *Phys. Rev. E* **2009**, *79*, 021404.
(40) Merabia, S.; Shenogin, S.; Joly, L.; Keblinski, P.; Barrat, J. L. Heat Transfer from Nanoparticles: A corresponding State Analysis. *Proc. Natl. Acad. Sci. U S A* **2009**, *106*, 15113−15118.

(41) Revised Release on the IAPS Formulation 1985 for the Viscosity of Ordinary Water Substance (International Association for the Properties of Water and Stream, 2003) http://www.iapws.org/.
(42) Toro, E. F. *Riemann Solvers and Numerical Methods for Fluid Dynamics*; Springer, Berlin, 1999.
(43) Kutateladze, S. S. *Fundamentals of Heat Transfer*; Academic Press, New York, 1963.
(44) Hu, M.; Hartland, G. *Ultrafast Dynamics of Metal Nanospheres and Nanorods*. In Nanoscale Materials. L. Liz-Marzán, P. Kamat, Eds.; Springer: New York, 2004; pp 97−118.
(45) Jain, P.; Lee, K.-S.; El-Sayed, I. H.; El-Sayed, M. A. Calculated Absorption and Scattering Properties of Gold Nanoparticles of Different Size, Shape, and Composition: Applications in Biological Imaging and Biomedicine. *J. Phys. Chem. B* **2006**, *110*, 7238−7248.
(46) Fang, Z.; Zhen, Y.-R.; Neumann, O.; Polman, A.; Garcia de Abajo, F. J.; Nordlander, P.; Halas, N. J. Evolution of Light-Induced Vapor Generation at a Liquid-Immersed Metallic Nanoparticle. *Nano Lett.* **2013**, *13*, 1736−1742.
(47) Link, S.; Burda, C.; Mohamed, M. B.; Nikoobakht, B.; El-Sayed, M. A. Laser Photothermal Melting and Fragmentation of Gold Nanorods: Energy and Laser Pulse-Width Dependence. *J. Phys. Chem. A* **1999**, *103*, 1165−1170.
(48) Habenicht, A.; Olapinski, M.; Burmeister, F.; Leiderer, P.; Boneberg, J. Jumping Nanodroplets. *Science* **2005**, *309*, 2043−2045.
(49) Petrova, H.; Hu, M.; Hartland, G. V. Photothermal Properties of Gold Nanoparticles. *Z. Phys. Chem.* **2007**, *221*, 361−376.
(50) Kurita, H.; Takami, A.; Koda, S. Size Reduction of Gold Particles in Aqueous Solution by Pulsed Laser Irradiation. *Appl. Phys. Lett.* **1998**, *72*, 789−791.
(51) Akchurin, G.; Khlebtsov, B.; Akchurin, G.; Tuchin, V.; Zharov, V.; Khlebtsov, N. Gold Nanoshell Photomodification under Single Nanosecond Laser Pulse Accompanied by Color-Shifting and Bubble Formation Phenomena. *Nanotechnology* **2008**, *19*, 015701.
(52) Werner, D.; Hashimoto, S. Controlling The Pulsed-Laser-Induced Size Reduction of Au and Ag Nanoparticles via Changes in The External Pressure, Laser Intensity, and Excitation Wavelength. *Langmuir* **2013**, *29*, 1295−1302.
(53) Cavicchi, R. E.; Meier, D. C.; Presser, C.; Prabhu, V. M.; Guha, S. Single Laser Pulse Effects on Suspended-Au-Nanoparticle Size Distributions and Morphology. *J. Phys. Chem. C* **2013**, *117*, 10866−10875.
(54) Lapotko, D.; Lukianova-Hleb, E.; Oraevsky, A. Clusterization of Nanoparticles During Their Interaction with Living Cells. *Nanomedicine* **2007**, *2*, 241−253.
(55) Chithrani, B. D.; Ghazani, A. A.; Chan, W. C. Determining The Size and Shape Dependence of Gold Nanoparticle Uptake Into Mammalian Cells. *Nano Lett.* **2006**, *6*, 662−668.
(56) Baffou, G.; Berto, P.; Bermúdez Ureña, E.; Quidant, R.; Monneret, S.; Polleux, J.; Rigneault, H. Photoinduced Heating of Nanoparticle Arrays. *ACS Nano* **2013**, *7*, 6478−6488.
(57) Yu, Y.-Y.; Chang, S.-S.; Lee, C.-L.; Wang, C. R. C. Gold Nanorods: Electrochemical Synthesis and Optical Properties. *J. Phys. Chem. B* **1997**, *101*, 6661−6664.
(58) Dickerson, E. B.; Dreaden, E. C.; Huang, X.; El-Sayed, I.; Chu, H.; Pushpanketh, S.; McDonald, J. F.; El-Sayed, M. Gold Nanorod Assisted Near-Infrared Plasmonic Photothermal Therapy (PPTT) of Squamous Cell Carcinoma in Mice. *Cancer Lett.* **2008**, *269*, 57−66.
(59) Garcia de Abajo, F. J. Colloquium: Light Scattering by Particle and Hole Array. *Rev. Mod. Phys.* **2007**, *79*, 1267−1290.
(60) Kravets, V. G.; Schedin, F.; Grigorenko, A. N. Extremely Narrow Plasmonic Resonances based on Diffraction Coupling of Lacalized Plasmons in Arrays of Metallic Nanoparticles. *Phys. Rev. Lett.* **2008**, *101*, 087403.
(61) Lapotko, D. O. Optical Excitation and Detection of Vapor Bubbles Around Plasmonic Nanoparticles. *Opt. Express* **2009**, *17*, 2538−2556.